Supplementary material:

MXenes: promising donor and acceptor materials for high-efficiency heterostructure solar cells

Yinggan Zhang[1], Rui Xiong[2], Baisheng Sa[2,*], Jian Zhou[3] and Zhimei Sun[3]

[1]*College of Materials, Fujian Provincial Key Laboratory of Theoretical and Computational Chemistry, Xiamen University, Xiamen 361005, P. R. China*
[2]*Key Laboratory of Eco-materials Advanced Technology, College of Materials Science and Engineering, Fuzhou University, Fuzhou 350108, P. R. China*
[3]*School of Materials Science and Engineering, and Center for Integrated Computational Materials Science, International Research Institute for Multidisciplinary Science, Beihang University, Beijing 100191, P. R. China*

Corresponding authors: *B. Sa: bssa@fzu.edu.cn.

Additional Theoretical methods

Formation and binding energy

To explore the thermodynamic stability of the heterostructures, the formation energy was defined as the following expression:[1]

$$E_{\text{form}} = E_{\text{Ti}_2\text{CO}_2/\text{M}_2\text{CO}_2} - E_{\text{Ti}_2\text{CO}_2} - E_{\text{M}_2\text{CO}_2} \quad (1)$$

where $E_{\text{Ti}_2\text{CO}_2/\text{M}_2\text{CO}_2}$ is the total energy of the Ti_2CO_2/M_2CO_2 (M=Zr and Hf) heterostructures, $E_{\text{Ti}_2\text{CO}_2}$ and $E_{\text{M}_2\text{CO}_2}$ represent the total energy of pristine Ti_2CO_2 and M_2CO_2 monolayers, respectively. In addition, we introduced the heterostructure binding energies to evaluate the strength of the vdW force in the Ti_2CO_2/M_2CO_2 heterostructures according to the equation:

$$E_{\text{binding}} = E_{\text{Ti}_2\text{CO}_2/\text{M}_2\text{CO}_2} - E_{\text{Ti}_2\text{CO}_2+\text{M}_2\text{CO}_2} \quad (2)$$

where $E_{\text{Ti}_2\text{CO}_2+\text{M}_2\text{CO}_2}$ is the sum of the total energies of the mutually independent Ti_2CO_2 and M_2CO_2 monolayers fixed in the corresponding heterostructure lattices.

Carrier mobility

The carrier mobility was explored on the basis of deformation potential theory as follows:[2,3]

$$\mu_{2\text{D}} = \frac{2e\hbar^3 C_{2D}}{3k_{\text{B}}T\,|m^*|\,E_{\text{i}}^2} \quad (3)$$

herein, the $C_{2\text{D}}$ is the elastic modulus and can be gotten *via* $C_{2D} = (\partial^2 E_{\text{total}} / \partial\varepsilon^2)/S_0$, where E_{total} is total energy shift with respect to the applied strain ε and S_0 is the area of the unit cell. Additionally, e, $\hbar$, k_{B} and T are the electron charge, reduced Planck

constant, Boltzmann constant and temperature, respectively. The temperature of 300 K was used in this work. The deformation potential constant E_i is defined as $E_i = \partial E_{edge} / \partial \varepsilon$, where E_{edge} is the band edge energy of the CBM for electrons and VBM for holes. The effective masses m^* was obtained by $m^* = \hbar^2(\partial E / \partial k^2)^{-1}$. The accuracy of mobility results calculated by PBE method have been proved by BeN_2,[4] TiS_3,[5] and *Pmma*-CO[6] in previous works. Thus, C_{2D}, E_i, and m^* were estimated by the PBE approach in this study.

Photocurrent

We have calculated the photocurrent of devices by first-order perturbation theory, which take the electron-photon interaction given by the Hamiltonian into consideration.[7-9] The device simulations were implemented in the QuantumWise Atomistix ToolKit (QuantumATK) Q2019.12 package.[10] The exchange and correctional interactions of electrons were described by the GGA-PBE form functional with a linear combination of atomic orbitals (LCAO) normconserving PseudoDojo pseudopotential.[11] A 0.3 V bias voltage was chose between the left (*L*) and right (*R*) electrodes for the photocurrent calculations. Herein, the applied bias voltage is much smaller than the band gaps of the MXene monolayers and heterostructures, so the calculated photocurrents are only generated by the light.[12,13] The results obtained by first-order perturbation theory have been proved to be consistent well with the experimental measurements of a silicon photovoltaic device.[14,15] After capture of *N* photons, photocurrent flow into the *L* and *R* electrodes, which can be defined as a function of frequency ω by the following expression:

$$I_\alpha = \frac{e}{h}\int_{-\infty}^{\infty} \sum_{\beta=L,R} [1 - f_\alpha(E)] f_\beta(E - h\omega) T^-_{\alpha,\beta}(E) - f_\alpha(E)[1 - f_\beta(E + h\omega)] T^+_{\alpha,\beta}(E) dE \quad (4)$$

$$T^{-}_{\alpha,\beta}(E)=N\ \mathrm{Tr}\left\{M^{\dagger}\hat{A}_{\alpha}(E)(MA_{\beta}(E-\hbar\omega)\right\} \quad (5)$$

$$T^{+}_{\alpha,\beta}(E)=N\ \mathrm{Tr}\left\{M\hat{A}_{\alpha}(E)(M^{\dagger}A_{\beta}(E+\hbar\omega)\right\} \quad (6)$$

where α ($\alpha \in L, R$) is electrode and f is the Fermi-Dirac distribution function of electrode. $A_{\alpha}=G\Gamma_{\alpha}G^{\dagger}$ is the spectral function of lead α, $\hat{A}_{\alpha}=G^{\dagger}\Gamma_{\alpha}G$ is the time-reversed spectral function of lead α, Γ_{α} is the spectral broadening, G and $G^{\dagger}$ are the retarded and advanced Green's functions, and the electron-photon coupling matrix is expressed as:

$$M_{\mathrm{ml}}=\frac{e}{m_0}\left(\frac{\hbar\sqrt{\hat{\mu}_r\hat{\varepsilon}_r}}{2N\omega\hbar}F\right)^{1/2}\mathbf{e}\cdot\ \mathbf{P}_{ml} \quad (7)$$

where $\mathbf{P}_{ml}$ is the momentum operator calculated by DFT-NEGF simulations.[16] Thus, the total photocurrent is the discrepancy between the L and R electrodes.

Table S1. Energy differences ΔE (meV) between various configurations and interlayer distances d (Å) for Ti_2CO_2/Zr_2CO_2 and Ti_2CO_2/Hf_2CO_2 heterostructures, as well as lattice constants a (Å) and bond lengths L (Å) for monolayers and heterostructures calculated by DFT-D3.

System	Configuration	ΔE	a	d	$L_{Zr/Hf-C}$	$L_{Zr/Hf-O}$	L_{Ti-C}	L_{Ti-O}
Ti_2CO_2			3.065				2.206	2.000
Zr_2CO_2			3.292		2.359	2.114		
Hf_2CO_2			3.250		2.356	2.098		
	a	0	3.199	2.361	2.324	2.085	2.259	2.038
	b	28.150	3.194	2.479	2.322	2.086	2.256	2.037
Ti_2CO_2/	c	118.011	3.190	2.990	2.321	2.086	2.255	2.037
Zr_2CO_2	d	122.023	3.190	3.018	2.321	2.086	2.255	2.038
	e	63.936	3.191	2.625	2.321	2.086	2.255	2.038
	f	26.871	3.194	2.481	2.322	2.085	2.256	2.038
	a	0	3.175	2.370	2.298	2.075	2.248	2.031
	b	37.113	3.171	2.424	2.296	2.075	2.247	2.031
Ti_2CO_2/	c	138.895	3.168	2.968	2.296	2.075	2.246	2.031
Hf_2CO_2	d	142.746	3.168	3.006	2.296	2.076	2.246	2.031
	e	78.696	3.169	2.598	2.296	2.076	2.246	2.031
	f	35.662	3.172	2.411	2.297	2.075	2.247	2.032

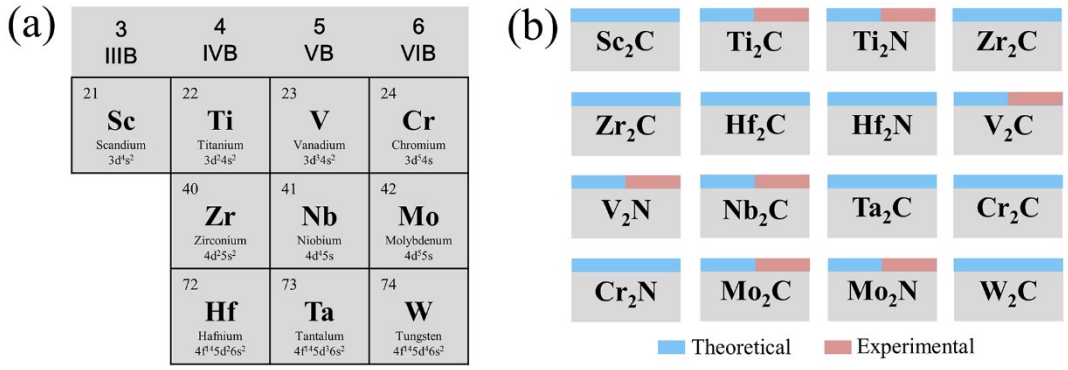

Fig. S1 (a) Position in the periodic table of M element for 2D MXenes. (b) Discovered theoretical and experimental M_2X-type MXenes so far.

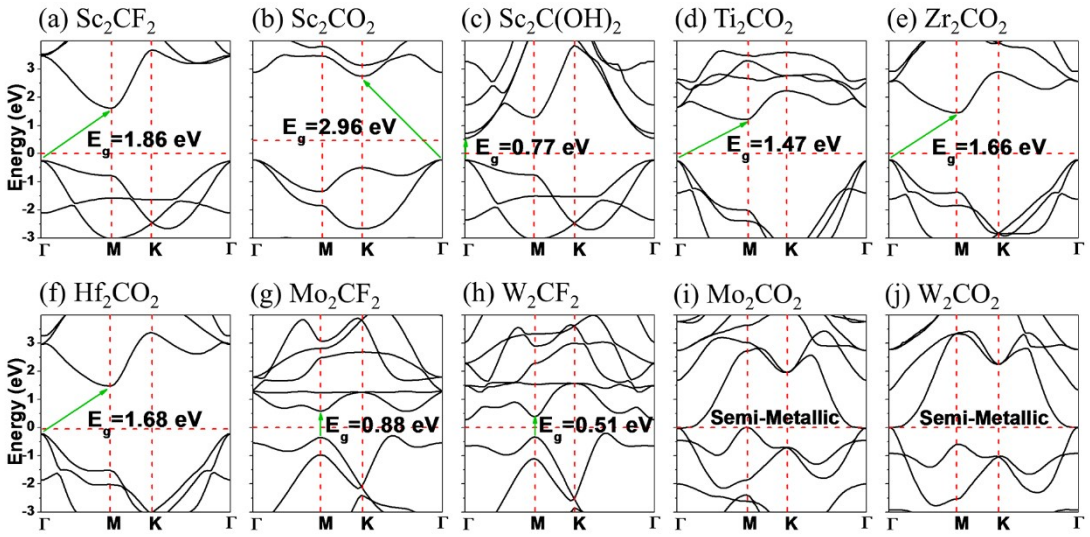

Fig. S2 The HSE06 band structures of the (a) Sc_2CF_2, (b) Sc_2CO_2, (c) $Sc_2C(OH)_2$, (d) Ti_2CO_2, (e) Zr_2CO_2, (f) Hf_2CO_2, (g) Mo_2CF_2, (h) W_2CF_2, (i) Mo_2CO_2, and (j) W_2CO_2 monolayers.

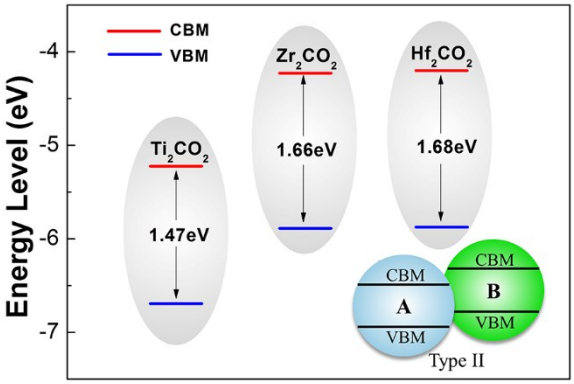

Fig. S3 (a) Band edge alignments for Ti_2CO_2, Zr_2CO_2, and Hf_2CO_2 monolayers. A type-II heterostructure is shown in the inset.

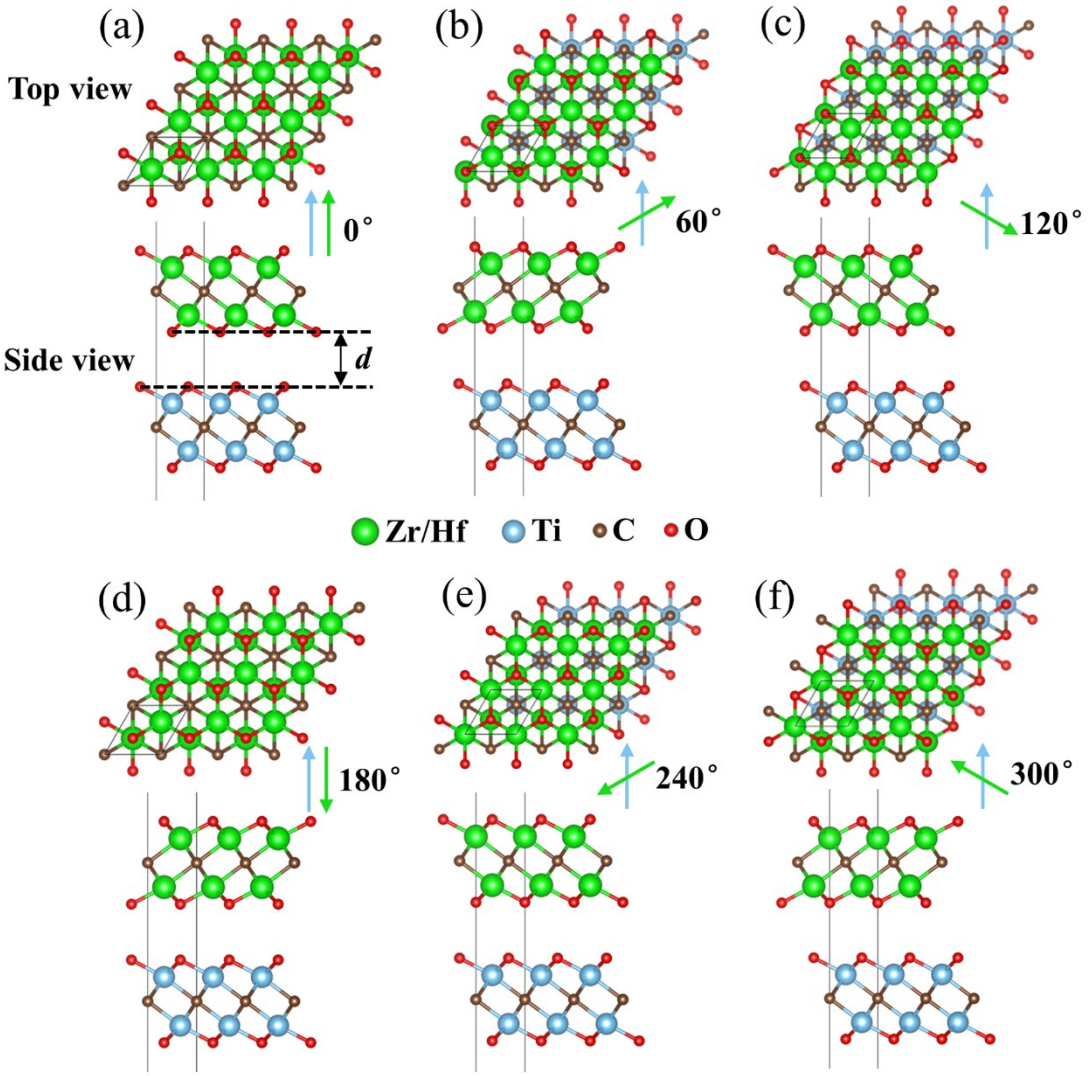

Fig. S4 Schematic views of the Ti_2CO_2/Zr_2CO_2 Ti_2CO_2/Hf_2CO_2 heterostructures with various configurations. The rotation angles of Zr_2CO_2 (Hf_2CO_2) monolayer with respect to Ti_2CO_2 are set to (a) 0°, (b) 60°, (c) 120°, (d) 180°, (e) 240°, and (f) 300°.

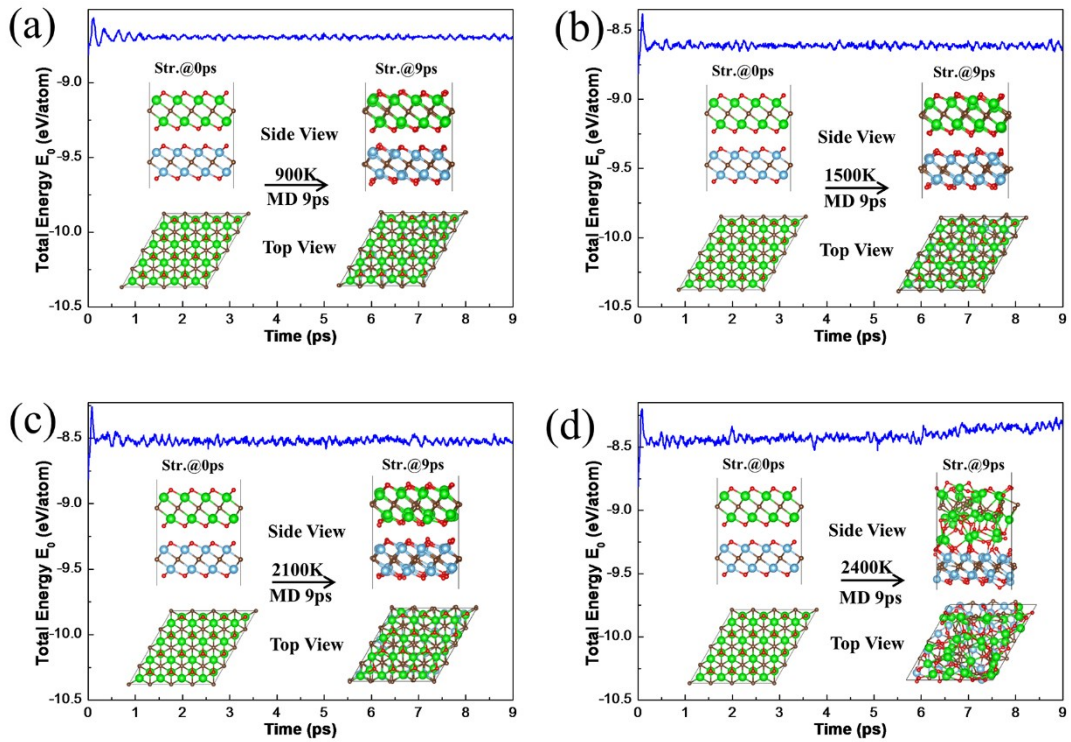

Fig. S5 The evolution of total energy and snapshots from AIMD simulations at 0 and 9 ps of Ti_2CO_2/Zr_2CO_2 heterostructure at (a) 900 K, (b) 1500 K, (c) 2100 K, and (d) 2400 K.

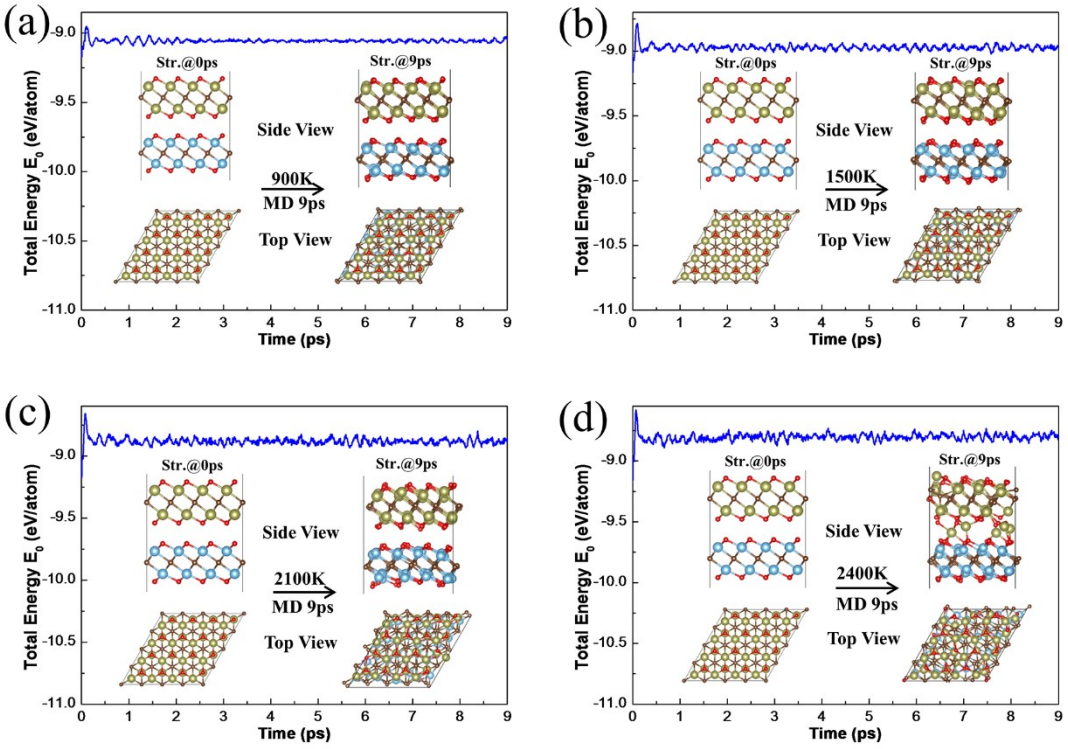

Fig. S6 The evolution of total energy and snapshots from AIMD simulations at 0 and 9 ps of Ti_2CO_2/Hf_2CO_2 heterostructure at (a) 900 K, (b) 1500 K, (c) 2100 K, and (d) 2400 K.

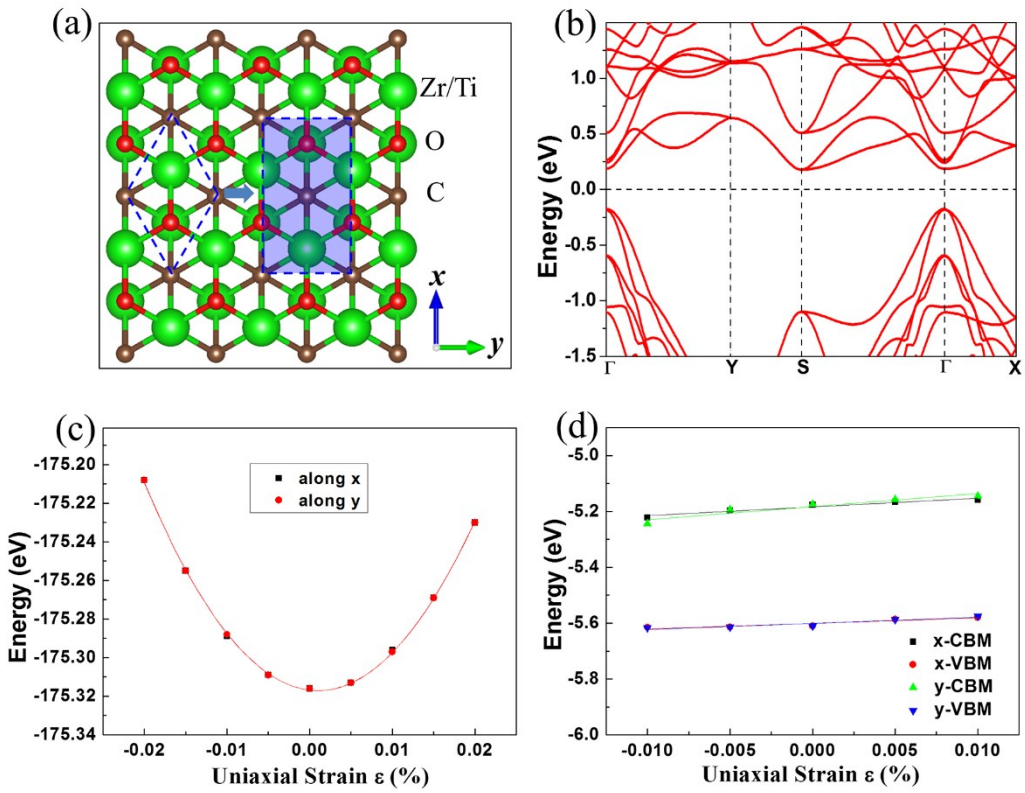

Fig. S7 (a) Top view of the atomic structure of Ti_2CO_2/Zr_2CO_2 heterostructure, here an orthorhombic lattice instead of hexagonal lattice was used. (b) Band structure of Ti_2CO_2/Zr_2CO_2 by PBE. (c) Total energy shift and (d) band edge positions of Ti_2CO_2/Zr_2CO_2 as a function of uniaxial strain along the *x* and *y* directions by PBE.

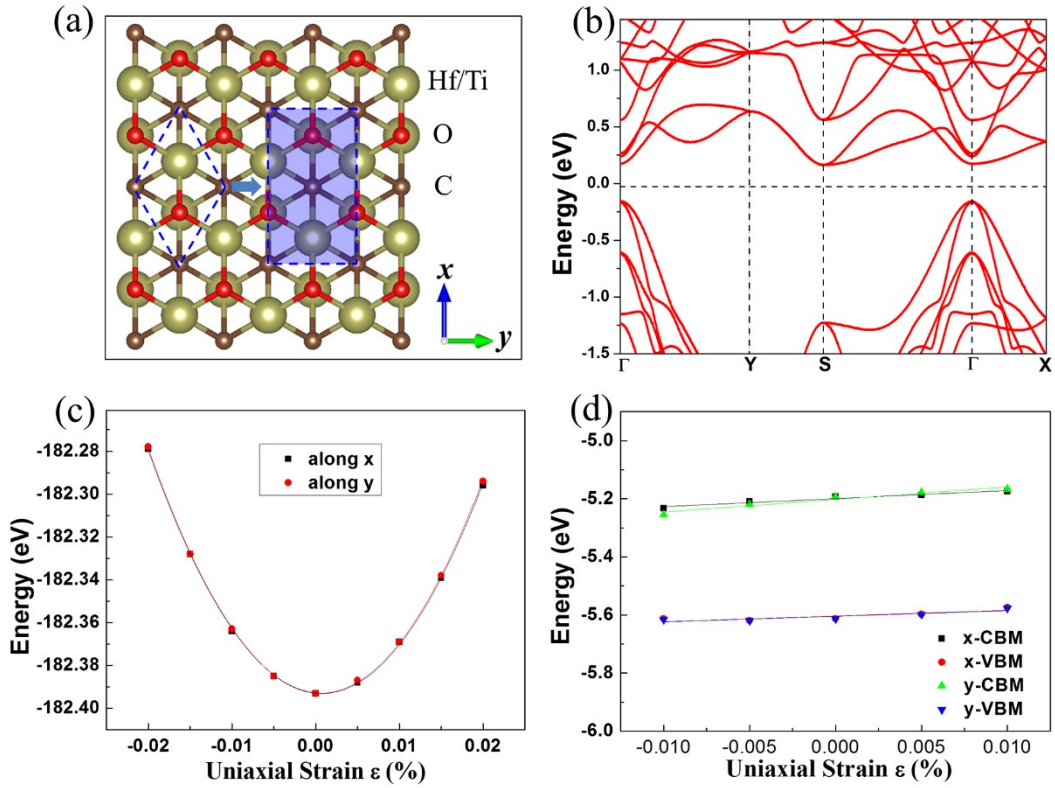

Fig. S8 (a) Top view of the atomic structure of Ti_2CO_2/Hf_2CO_2 heterostructure, here an orthorhombic lattice instead of hexagonal lattice was used. (b) Band structure of Ti_2CO_2/Hf_2CO_2 by PBE. (c) Total energy shift and (d) band edge positions of Ti_2CO_2/Hf_2CO_2 as a function of uniaxial strain along the *x* and *y* directions by PBE.

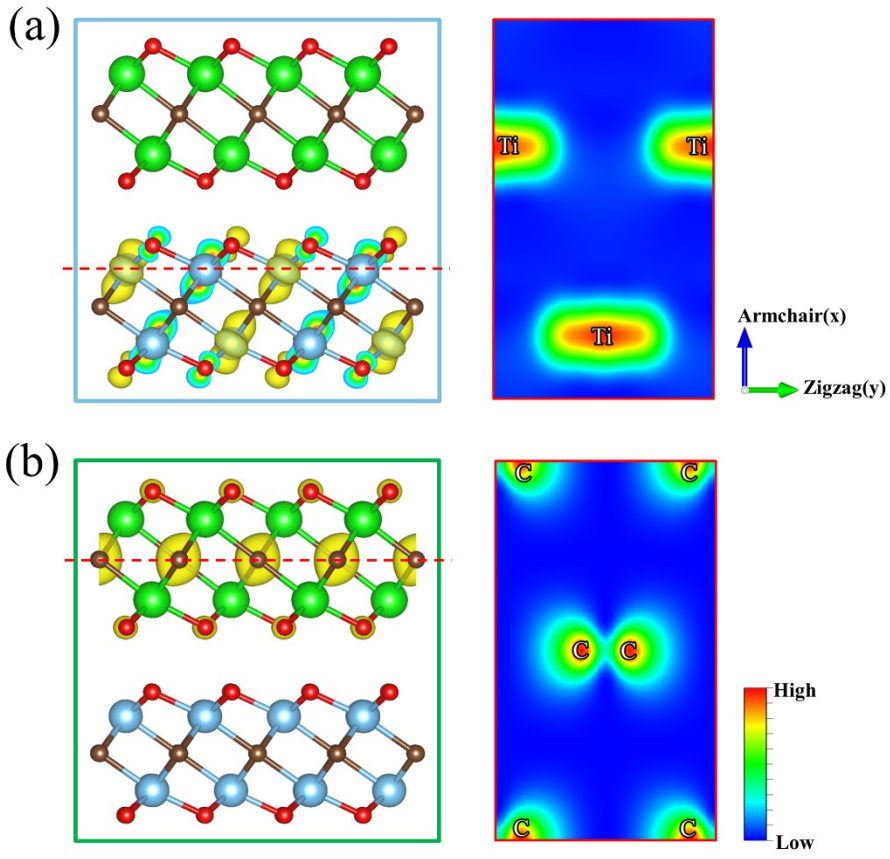

Fig. S9 Band-decomposed charge density of the (a) CBM and (b) VBM for Ti_2CO_2/Zr_2CO_2 heterostructure in the orthorhombic lattice. The right part is the 2D charge density picture in the *xy*-plane, the location of which is marked with a red dashed line in the left part.

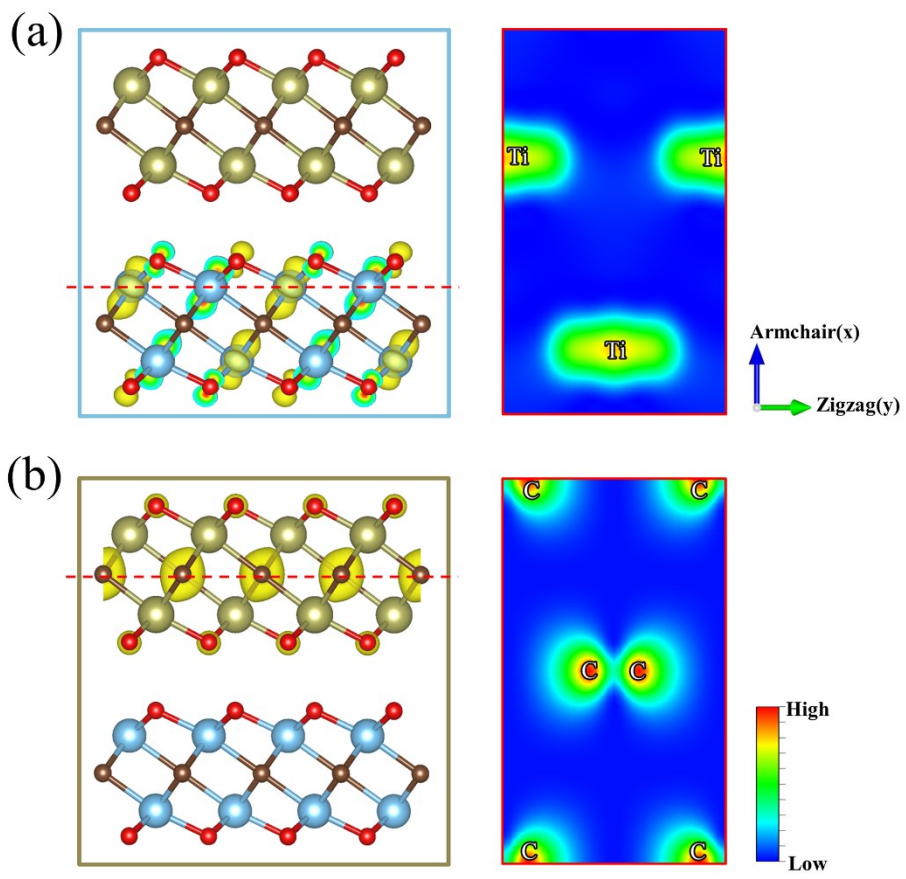

Fig. S10 Band-decomposed charge density of the (a) CBM and (b) VBM for Ti_2CO_2/Hf_2CO_2 heterostructure in the orthorhombic lattice. The right part is the 2D charge density picture in the *xy*-plane, the location of which is marked with a red dashed line in the left part.

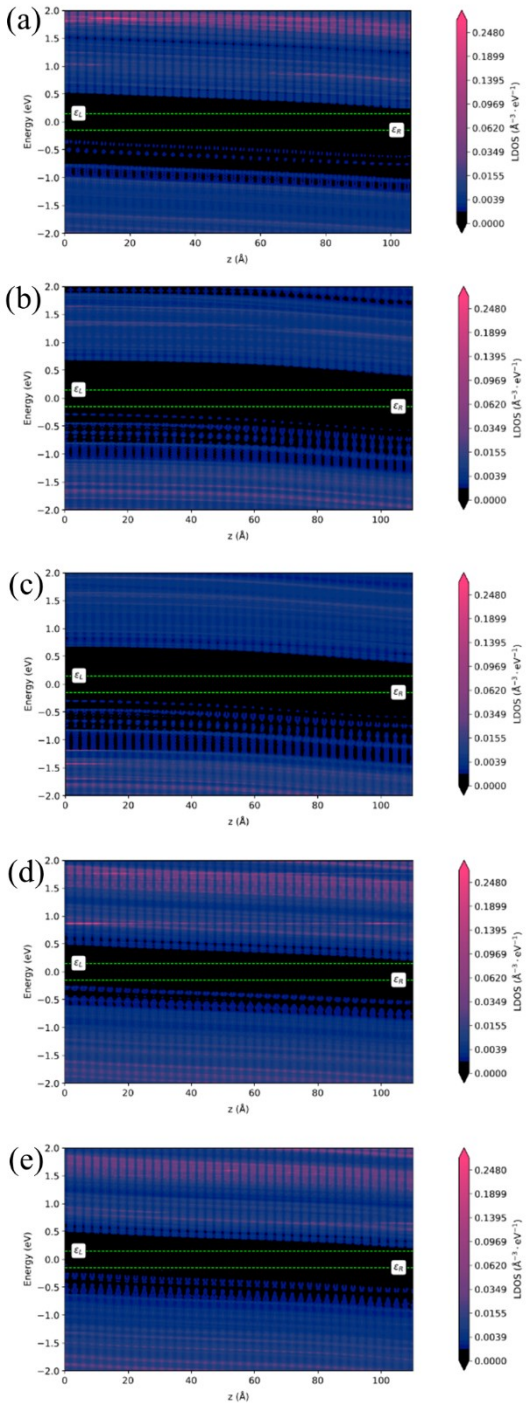

Fig. S11 Local density of states along the transport direction of (a) Ti_2CO_2, (b) Zr_2CO_2, (c) Hf_2CO_2, (d) Ti_2CO_2/Zr_2CO_2, and (e) Ti_2CO_2/Hf_2CO_2 solar cell devices.

References

1. Q. Peng, K. Hu, B. Sa, J. Zhou, B. Wu, X. Hou and Z. Sun, *Nano Res.*, 2017, **10**, 3136-3150.
2. J. Qiao, X. Kong, Z.-X. Hu, F. Yang and W. Ji, *Nat. Commun.*, 2014, **5**, 4475.
3. Q. Peng, R. Xiong, B. Sa, J. Zhou, C. Wen, B. Wu, M. Anpo and Z. Sun, *Catal. Sci. Technol.*, 2017, **7**, 2744-2752.
4. C. Zhang and Q. Sun, *J. Phys. Chem. Lett.*, 2016, **7**, 2664-2670.
5. J. Dai and X. C. Zeng, *Angew. Chem. Int. Ed.*, 2015, **54**, 7572-7576.
6. Z.-W. Teng, C.-S. Liu and X.-H. Yan, *Nanoscale*, 2017, **9**, 5445-5450.
7. J. Z. Chen, Y. B. Hu and H. Guo, *Phys. Rev. B*, 2012, **85**, 155441.
8. C. Rivas, R. Lake, G. Klimeck, W. R. Frensley, M. V. Fischetti, P. E. Thompson, S. L. Rommel and P. R. Berger, *Appl. Phys. Lett.*, 2001, **78**, 814-816.
9. J. Wang, H. Guo, J. J. Xue, D. J. Chen, G. F. Yang, B. Liu, H. Lu, R. Zhang and Y. D. Zheng, *Sol. RRL*, 2019, **3**, 1-5.
10. S. Smidstrup, T. Markussen, P. Vancraeyveld, J. Wellendorff, J. Schneider, T. Gunst, B. Verstichel, D. Stradi, P. A. Khomyakov, U. G. Vej-Hansen, M.-E. Lee, S. T. Chill, F. Rasmussen, G. Penazzi, F. Corsetti, A. Ojanperä, K. Jensen, M. L. N. Palsgaard, U. Martinez, A. Blom, M. Brandbyge and K. Stokbro, *J. Phys.: Condens. Matter*, 2019, **32**, 015901.
11. V. Blum, R. Gehrke, F. Hanke, P. Havu, V. Havu, X. G. Ren, K. Reuter and M. Scheffler, *Comput. Phys. Commun.*, 2009, **180**, 2175-2196.
12. L. Zhang, K. Gong, J. Chen, L. Liu, Y. Zhu, D. Xiao and H. Guo, *Phys. Rev. B*, 2014, **90**, 195428.
13. Y. Liang, Y. Dai, Y. Ma, L. Ju, W. Wei and B. Huang, *J. Mater. Chem. A*, 2018, **6**, 2073-2080.
14. M. Palsgaard, T. Markussen, T. Gunst, M. Brandbyge and K. Stokbro, *Phys. Rev. Appl.*, 2018, **10**, 014026.
15. B. J. Huang, P. E. Yang, Y. P. Lin, B. Y. Lin, H. J. Chen, R. C. Lai and J. S. Cheng, *Sol. Energy*, 2011, **85**, 388-392.
16. M. Brandbyge, J.-L. Mozos, P. Ordejón, J. Taylor and K. Stokbro, *Phys. Rev. B*, 2002, **65**, 165401.